Melting and Crystallization of Polyethylene of Different Molar Mass by Calorimetry†

Jeongihm Pak and Bernhard Wunderlich*

Department of Chemistry, The University of Tennessee, Knoxville, Tennessee 37996-1600, and Chemical and Analytical Sciences Division, Oak Ridge National Lab., Oak Ridge, Tennessee 37831-6197

Received February 2, 2001; Revised Manuscript Received April 17, 2001

ABSTRACT: Crystallization and melting of *n*-paraffins of chain lengths up to $C_{60}H_{122}$ can be largely reversible, and practically no supercooling is seen in differential scanning calorimetry (DSC) and temperature-modulated DSC (TMDSC). To find the changes with chain length for this effect, polyethylene fractions of oligomers of mass 560, 1150, and 2150 Da and a polymer of mass 15 520 Da were analyzed. The mode of analysis was quasi-isothermal TMDSC with an amplitude of 0.5 K about a fixed series of temperatures. For the oligomer of 560 Da, a mainly reversing melting was seen, similar to the behavior of paraffins of the same molar mass. The oligomer of 2150 Da as well as the polymer shows an irreversible crystallization with a crystallization of more than 5.0 K below the melting temperature, and the oligomer of 1150 Da is intermediate. Typical for polymers, a small amount of reversing material remains in the melting range of the polymer. The 1150 and the 2150 Da oligomers grow to extended-chain crystals, and the polymer yields folded-chain crystals. This research reveals that there is little difference in reversibility between monodisperse paraffins and fractions with similar average mass. There is no major difference in supercooling behavior for extended- and folded-chain crystals. The critical chain length for which a substantial supercooling is observed is 12.5 nm. The three types of reversible latent heat observed in macromolecules are traced to the short-chain molecules.

Introduction

It is well-known that flexible linear macromolecules (usually just called polymers) do not crystallize at the temperature where they melt, even if the melt or solution is nucleated by seeding or self-seeding.[1] Polymers usually need a 5−30 K supercooling to crystallize.[2] Experiments approaching homogeneous nucleation with dispersions of small droplets need even larger supercoolings, of the order of 50−140 K.[2] To rationalize that even in the presence of primary nuclei and crystal surfaces polymer melts and solutions supercool, a second barrier to crystallization is assumed.

The term supercooling is in this connection defined as the temperature difference between zero-entropy production melting and first observed crystallization. Naturally, the first observed crystallization is time-dependent, but the increasing time needed for initial crystal growth at higher temperature is exponential and reaches quickly experimentally unreasonable values.[1] In addition, the thermodynamic condition of zero-entropy production melting must be specified since it applies to two cases: The first case is the well-known equilibrium, given by $\Delta G_f° = 0 = \Delta H_f° - T_m°\Delta S_f°$, where $T_m°$ is the equilibrium melting temperature. The second case applies to melting from a metastable crystal to an equally metastable melt. This case is common in the melting of chain-folded crystals where reorganization is avoided either by fast melting or by immobilizing the amorphous fraction.[3] The description is based on the Gibbs−Thomson equation and can be written for chain-folded crystals as $\Delta G_f° - A\gamma = 0 = (\Delta H_f/T_m°)(T_m° - T_m)$, where A is the fold-surface area, γ is the appropriate surface free energy, T_m is the zero-entropy production melting temperature, and ΔH_f is the heat of fusion at T_m, usually only little different from $\Delta H_f°$. This analysis using irreversible thermodynamics is known for many years[4] and has been applied to many polymers.[3]

We expect that each amorphous polymer molecule must traverse many cooperative steps of conformational motion before ordering to the macroconformation[5] that adds to the existing crystal growth face. To describe this initial stage of crystallization of the polymer in the presence of primary nuclei, the term molecular nucleation was coined.[2,6,7] Only few details of molecular nucleation, however, have emerged over the past 20 years.[8,9] Most important, in addition to the supercooling behavior, is the observation that segregation of molecules of lower masses on crystallization can occur below the equilibrium melting temperature of the rejected species. This is only possible if there is another reversible process other than the equilibrium crystallization and melting to achieve such segregation. We suggested that molecular nucleation is such a process, although the detailed mechanism is not known.[10]

The invention of temperature-modulated differential scanning calorimetry (TMDSC)[11−13] provides a new tool to search for reversible processes during the melting and crystallization of polymers. Indeed, several years ago, in addition to the mainly irreversible processes, a small reversible component was discovered in the melting region of polymers.[14−17] This paper is a further effort to study reversible melting on the example of polyethylene and its oligomers and to establish a link to the properties of paraffins. For paraffins melting and crystallization is largely reversible within the modulation amplitude of the calorimetry. With increasing chain length, however, the melting and crystallization becomes irreversible, with local equilibria remaining within the metastable superstructure of the crystalline and mobile as well as rigid−amorphous fractions. In addition, annealing of the crystalline and amorphous

† This work was presented in part at the 28th NATAS Conference in Orlando, FL, Oct 4−6, 2000.

10.1021/ma010195a CCC: $20.00
Published on Web 05/25/2001

superstructure may occur during the calorimetric analysis and affect the local equilibria. The calorimetric analysis of these complicated chains of events can be separated into the "total" changes, which correspond ideally to the scanning calorimetry without temperature modulation, and the "reversing" changes, which are following a modulation of the temperature. By extending the time of analysis on modulation about a constant temperature by performing a quasi-isothermal analysis, truly "reversible" local or global processes can be identified as soon as the response to the modulation becomes identical for successive oscillations in temperature. Special problems that arise from the inevitable calorimeter lags and the time spans needed for the deconvolution of the data in the frequency domain have been studied recently[18] and need to be accounted for.

Temperature-modulated DSC with varying amplitudes has been used earlier as a tool to study well- and poorly-crystallized poly(oxyethylene)s (POE) of 1500, 4540, and 35 000 Da molar mass.[16,17] Irreversible processes and an additional, small amount of reversing melting and crystallization were identified. These results will also be included in the present discussion. The *n*-paraffins $C_{50}H_{102}$ and $C_{60}H_{122}$ were then chosen as simple model compounds for polyethylene. Unexpectedly, however, these paraffins and the lower homologues, $C_{44}H_{90}$ and $C_{26}H_{54}$, did not show supercooling on crystallization from the melt.[19,20] Also, in a recent study of the heterogeneous and homogeneous nucleation of *n*-alkanes by Sirota et al., [21−23] such results were reported for *n*-paraffins with $21 \leq n \leq 37$ carbon atoms. The same authors reported an about 15 K supercooling before homogeneous nucleation of paraffins is possible. This is much smaller than the degree of supercooling of 50 K needed for homogeneous nucleation of polyethylene, which in turn is less than the supercooling of most other polymers analyzed.[2] All these observations indicate that the study of crystallization and melting by temperature-modulated calorimetry may shed some light on the nucleation and growth process of crystals of polyethylene. Of present interest is to establish the chain length for the onset of supercooling and to learn more about the locally reversible processes.

Experimental Section

Apparent heat capacity measurements were carried out with a Thermal Analyst 2920 MDSC from TA Instruments Inc., an isoperibol heat-flux twin calorimeter with modulation control by the sample-temperature sensor. Dry N_2 gas with a flow rate of 20 mL min^{-1} was purged through the differential scanning calorimeter. A refrigerated cooling system (RCS; cooling capacity to 220 K) was used. The temperature of the equipment was initially calibrated in the standard differential scanning calorimetry mode (DSC), using the onset temperatures of the melting transition peaks for water (273.15 K), indium (429.75 K), and tin (505.08 K) at a scanning rate of 10 K min^{-1}. The heat flow rate was calibrated with the specific heat of fusion of indium (28.45 J g^{-1}). The melting temperature of In was also measured in the quasi-isothermal mode of TMDSC with a 0.05 K modulation amplitude after the calibration in the standard DSC mode to identify any differences between two modes of measurement. In the standard DSC mode, the onset melting temperature of indium, a secondary temperature standard, was set to its value of 429.75 K at 10 K min^{-1}. It was found then that a quasi-isothermal TMDSC experiment led to a melting temperature of 429.31 K. To correct the sample temperatures of the quasi-isothermal measurements, we added the difference of 0.40 K as a calibration constant to the average temperatures of the quasi-isothermal measurements at T_0. The change of the onset temperature of melting with the rate of heating is approximately 0.03 K per K min^{-1}, which can account for most of this temperature difference.

Table 1. Molar Masses, Chain Lengths, and Melting Temperatures of Paraffins, Polyethylenes, and Poly(oxyethylene)

samples	no. of backbone atoms	molar mass (Da)	chain length (nm)	equilib temp[a] (K)
n-$C_{26}H_{54}$	26	366.70	3.16	$T_i = 329.5$
n-$C_{44}H_{90}$	44	619.20	5.44	$T_m = 359.6$
n-$C_{50}H_{102}$	50	703.37	6.20	$T_m = 365.3$
n-$C_{60}H_{122}$[b]	60	843.64	7.46	$T_m = 372.9$
PE560	40	560	4.9	$T_m = 354.5$
PE1150	82	1150	10.2	$T_m = 383.3$
PE2150	153	2150	19.2	$T_m = 397.2$
PE15520	1106	15520	140	$T_m = 411.9$
PE130000[c]	9266	130000	1172	$T_m = 413.4$
POE1500	102	1500	9.4	$T_m = 322.3$
POE1960[b]	133	1960	12.3	$T_m = 326.5$
POE3060[b]	208	3060	19.2	$T_m = 331.7$
POE5000	309	4540	28.4	$T_m = 333.8$

[a] Melting temperatures, T_m, and the isotropization temperature, T_i, for paraffins and PE samples refer to values calculated from eq 2. The disordering temperature, T_d, of *n*-$C_{26}H_{54}$ from the orthorhombic to the conformationally disordered crystal (the "rotor phase") occurs at 326.5 K. On cooling, this transition supercools by 4.0 K, while T_i is close to reversible. The TMDSC of POE1500 and POE5000 have been studied earlier,[16,17] and the POE equilibrium melting temperatures are computed from literature data.[3,25] The supercoolings, if not stated otherwise, are measured from the zero-entropy-production melting temperatures which are somewhat lower for the paraffins than given in this table and much lower for the high-molar-mass polyethylenes which chain-fold. [b] Thesis, J. Pak, Department of Chemistry, The University of Tennessee, Knoxville, TN, 2001. [c] Earlier data on linear PE of polydispersity 13.[1]

Quasi-isothermal TMDSC was done with a sinusoidal modulation period of 60 s, a modulation amplitude of 0.5 K, and stepwise temperature increments of T_0 of 1−5 K, depending on the changes expected in the sample response. The last 10 min of the 20 min quasi-isothermal runs was used for data collection to calculate the reversing heat capacity C_p as follows:[24]

$$C_p = \frac{A_\Phi}{A_{T_s}\omega} K' \tag{1}$$

where A_Φ is the amplitude of the heat-flow rate and A_{T_s} is the amplitude of the temperature modulation. Both amplitudes are calculated as the first harmonics of the Fourier series describing the heat-flow rate and the sample temperature. The frequency in rad s^{-1} is given by ω, and K' represents the calibration constant at the given conditions of measurement. The crystallinity of the samples was determined from the heat of fusion measured by standard DSC on heating at 10 K min^{-1} prior to and after the quasi-isothermal measurements.

The polyethylene samples named PE560, PE1150, PE2150, and PE15520 were purchased from Scientific Polymer Products Inc. Their weight-average molar masses were 560, 1,150, 2,-150, and 15 520 Da and M_w/M_n was listed as 1.09, 1.20, 1.15, and 1.08, respectively. These and all samples discussed in this paper are compared in Table 1. Samples of 0.53−1.07 mg were weighed on a Cahn C-33 electrobalance to an accuracy of ±0.001 mg and encapsulated in standard aluminum pans (23 mg, including a cover). A somewhat lighter reference pan of 22 mg was used for all measurements to correct easily for the asymmetry of the calorimeter by adding the reversing heat capacity from eq 1 for a run with an empty sample pan and the lighter reference pan.[26]

Results

Standard DSC. Figure 1 contains a plot of the peak temperatures of crystallization and melting of the

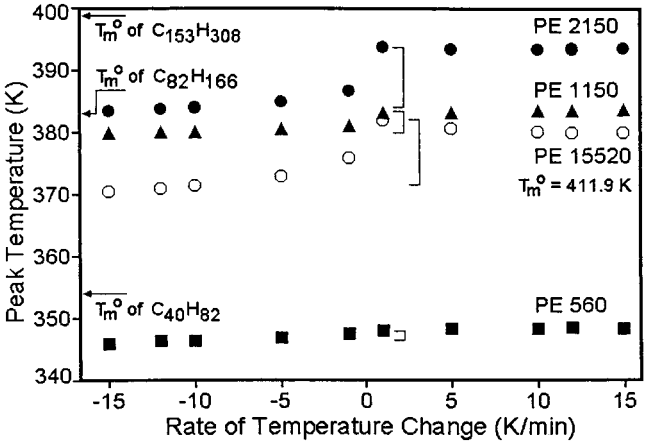

Figure 1. Temperatures of crystallization and melting peaks as a function of scanning rates when measured by standard DSC.

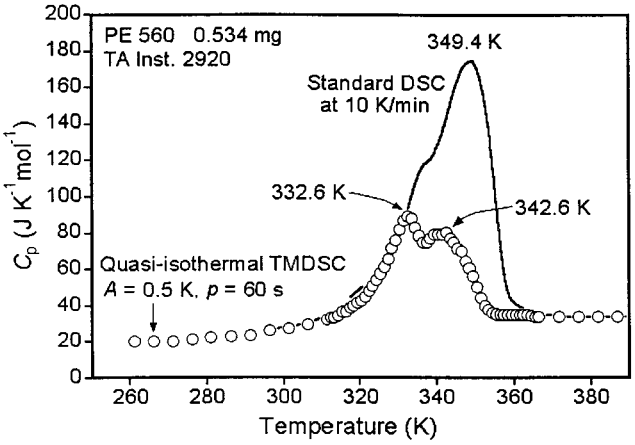

Figure 2. Apparent heat capacities measured by standard DSC and quasi-isothermal TMDSC for PE560 crystallized first from the melt on cooling at 10 K min^{-1}. The solid line is obtained by standard DSC at 10 K min^{-1} and the open circles represent the apparent, reversing heat capacity by quasi-isothermal measurements.

oligomers and the polymer of this research as a function of the scanning rate when measured by standard differential scanning calorimetry (DSC). The peak temperatures of melting of PE560 are somewhat less than 354.5 K, the equilibrium melting temperature, $T_m°$, of $C_{40}H_{42}$, as calculated from the empirical equation of Broadhurst[27] which fits the experimental data from $C_{11}H_{24}$ to $C_{100}H_{202}$ with a root-mean-square deviation of ±0.41 K:[3]

$$T_m° = \frac{414.3(x - 1.5)}{x + 5.0} \qquad (2)$$

with x representing the number of carbon atoms in the *n*-paraffin. The number-average molar mass of PE560 corresponds to $C_{37}H_{76}$ which has according to eq 2 a $T_m°$ of 350.2 K. Between the data taken on heating and cooling there is at best a small indication of supercooling which is further investigated below by using quasi-isothermal TMDSC. Because of the molar mass distribution in PE560, one might assume that the smallest crystals melt first, but the largest molecules crystallize first, complicating the quantitative interpretation of the melting peaks that lead to Figure 1.

The melting and crystallization temperatures of the longer polyethylene oligomers, PE1150 and PE2150, are also shown in Figure 1. In contrast to PE560, there is an increasing supercooling in these samples, as indicated by the mark]. The PE1150 is expected to have an equilibrium melting temperature of 383.3 K, PE2150, of 397.2 K, which are extrapolated from eq 2 and are not far from the observed value, as marked in Figure 1. The melting temperature of PE15520, in contrast, is about 30 K lower than that expected for an equilibrium crystal of polyethylene of its molar mass with an extended-chain macroconformation and is even approximately 13 K lower than that for PE2150, although PE15520 is 7 times longer than PE2150. Chain folding, which has been observed for chain lengths longer than 37 nm,[28,29] is the main reason for the large difference between the expected and measured melting temperature of PE15520.[3] Of importance for the further discussion is that both the chain-folded PE15520 and the extended-chain PE2150 show similar supercoolings of almost 10 K, compared to almost none, for the paraffins[19,20] and the PE560.

TMDSC of PE560. Figure 2 displays the results of measurements by standard DSC and quasi-isothermal TMDSC of melt-crystallized PE560. The apparent total C_p by standard DSC, run prior to the quasi-isothermal measurements, is measured with a heating rate of 10 K min^{-1} and is indicated by the solid line. In this figure, and all subsequent ones, the mole in the dimension of the heat capacity refers to one CH_2 group; i.e., it is 14.03 Da. The open circles are the apparent, reversing heat capacities, obtained from the subsequent quasi-isothermal TMDSC at increasing temperatures. The crystallinity was determined by standard DSC using the heat of fusion at the average temperature of measurement.[3] It was 70% at room temperature after cooling at 10 K min^{-1} and improved to 82% after the long-time, quasi-isothermal runs on cooling in steps of different values of T_0 which permit increased annealing. The two peaks in the melting curve are not clearly separated in the standard DSC run but are revealed more clearly in the TMDSC runs. The melting temperature of 354.5 K for $C_{40}H_{82}$ with a similar molar mass to PE560 approximates the higher temperature peak. The first peak is most likely the eutectic separation of the different mass crystals and may contain some of the transition to a high-temperature mesophase, observed in paraffins with a lower mass than $C_{40}H_{82}$. The apparent reversing heat capacity plot shows a sizable contribution to the melting but not as much as seen for the pure $C_{50}H_{102}$ which crystallizes reversibly to almost 100%. When measured by quasi-isothermal TMDSC with an amplitude of 0.05 K, 66% of the total crystals of $C_{50}H_{102}$ melt within 0.1 K or less, and all fusion is complete within 1.0 K;[19] i.e., with the present, larger modulation amplitude of 0.5 K, the melting would have been practically fully reversing. The width of the region of melting of PE560 is more than 30 K, and the maximum in the reversing C_p reaches only half the C_p of the melting peak by standard DSC. The broadening of the melting of PE560 in the quasi-isothermal measurements is, thus, most likely due to the chain-length distribution. The additional shift to higher temperature in the standard DSC experiment for the high-temperature portion of the melting peak and the end of melting is due to the thermal lag of the calorimeter when heated at 10 K min^{-1} through the melting region.[18]

In Figure 3, the experiment of Figure 2 is continued by quasi-isothermal measurements with decreasing

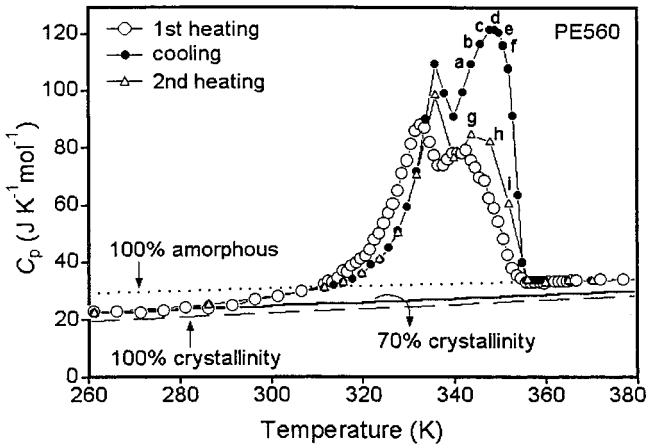

Figure 3. Apparent, reversing heat capacities of PE560 on heating and cooling by quasi-isothermal TMDSC. Open circles, filled circles, and triangles represent the first heating, subsequent cooling, and the second heating, respectively (see also Figure 2).

temperatures starting from the melt, followed by a subsequent second heating run. The apparent reversing heat capacities are plotted as a function of temperature, as before, and can be compared quantitatively to the heat capacity of an amorphous, crystalline, and 70% crystalline sample, as derived from the ATHAS data bank excluding any melting and crystallization contributions.[30] Both quasi-isothermal heating runs show that the end of melting occurs at 355 K. The quasi-isothermal cooling run after the first heating proves that the beginning of crystallization occurs also at 355 K. A second cooling run is not depicted in Figure 3, but it was identical to the first. There is no supercooling of PE560 in the quasi-isothermal TMDSC experiments with 0.5 K of amplitude. The shifts of the peak positions between first and second heating runs can be explained by changes in the cocrystallization of different chain lengths and perfection in the crystal morphology, as is also indicated by the increase in the overall crystallinity mentioned above.

The higher apparent reversing heat capacities in the regions of the points marked a−f in the cooling sequence relative to g−i in the heating sequence are analyzed in the more detailed graphs in Figure 4. Corresponding data for the marked points are given in the graphs for the modulation of the temperature (bottom), the total heat flow rate (center), and the apparent, reversing, specific heat capacity (top). After attainment of steady state, the specific heat capacity continues to decrease at the temperatures from f−a and drifts toward the measurements on heating at points g−i which show a constant reversing heat capacity in each run after about 10 min.

TMDSC of PE1150 and PE2150. Figure 5 represents the results for PE 1150 and PE2150. Again, the thick, continuous solid line is the apparent total C_p from the standard DSC, carried out prior to the quasi-isothermal TMDSC measurements. The open circles are the apparent reversing C_p obtained from the first quasi-isothermal heating TMDSC runs. The peak temperature of the standard DSC run is close to the equilibrium melting temperatures of $C_{82}H_{166}$ and $C_{153}H_{308}$ (see Figure 1). The crystallinities are 83 and 89%, calculated from the heat of fusion obtained from the standard DSC run, and the melting ranges are both about 30−40 K wide (see also Figure 6), although the main melting

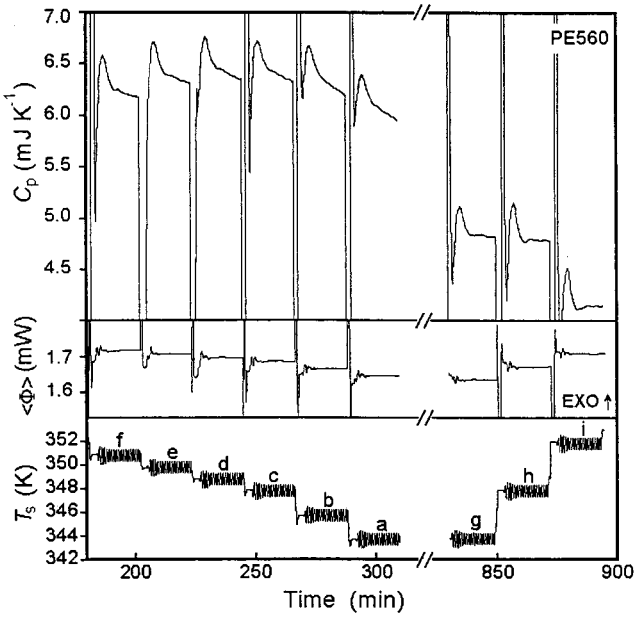

Figure 4. Detailed analysis in the region of the reversing melting peak of PE560. Apparent reversing heat capacity, total heat-flow rate ⟨Φ⟩, and sample temperature $T_s(t)$ during cooling and subsequent heating. Corresponding points to Figure 4 are marked.

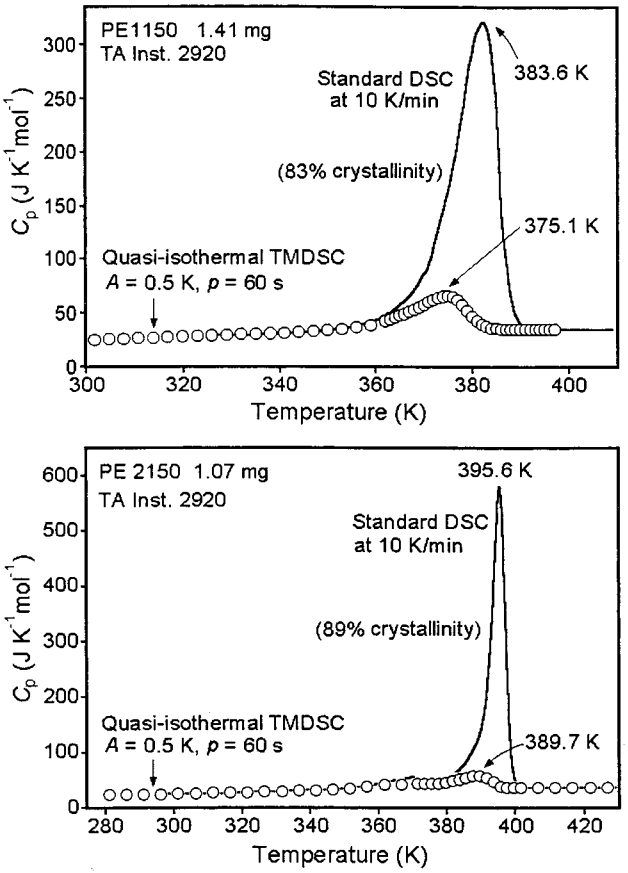

Figure 5. Apparent heat capacities measured by standard DSC and quasi-isothermal TMDSC for PE 1150 (a) and PE2150 (b) after crystallization from the melt with a cooling rate of 10 K min^{-1}. The solid line is obtained by standard DSC at 10 K min^{-1} and the open circles represent the apparent, reversing heat capacities by quasi-isothermal measurements.

peaks narrow and become of higher amplitude with molar mass. The apparent reversing heat capacity plots shows only a very small contribution to melting. The

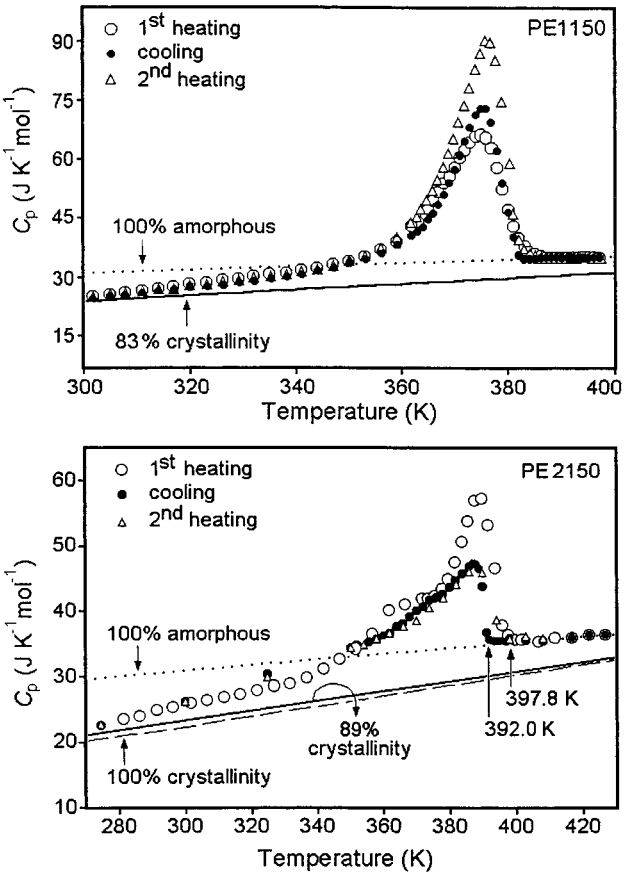

Figure 6. Apparent, reversing heat capacities of PE1150 (a) and PE2150 (b) on heating and cooling by quasi-isothermal TMDSC. The first heating corresponds to an enlargement of the quasi-isothermal run shown in Figure 5.

shallow peak for PE2150 at about 370 K in the standard DSC trace is largely irreversible; i.e., it is very much reduced in quasi-isothermal TMDSC. Enlarging the ordinate, as shown in Figure 6b, reveals that the remaining 370 K peak on first heating disappears fully on cooling and does not reappear on the second heating, after better crystallization was possible on cooling under TMDSC conditions. No further discussion will be given about this irreversible melting peak which was induced by the initial, 10 K min^{-1} cooling.

Figure 6 displays the reversing heat capacity plots of PE1150 and PE2150 as a function of temperature, as described in Figure 3 for PE560. The second cooling runs were identical to the first and are not depicted in Figure 6. The dashed line in Figure 6b is the C_p for 100% crystalline PE without latent heat contributions, and the dotted lines in Figure 6a,b are for 100% amorphous samples, as given in the ATHAS data bank.[30] The solid lines are computed for the 83% and 89% crystalline samples, as measured by standard DSC in parts a and b of Figure 5. For PE1150 shown in Figure 6a, the end of melting on first heating is at 386.2 K and the onset of crystallization on cooling is 382.1.0 K. The difference of about 4.1 K represents the supercooling. For PE2150 the end of melting on first and second heating is at 397.8 and 397.9 K, respectively, and the onset of crystallization on first and second cooling is 392.0 K. The difference of about 5.8 K represents the supercooling of PE2150. For PE2150 the apparent reversing plots of C_p on cooling and on second heating are matched from low temperature to the temperature of the maximum. For PE1150 the maximum on cooling is still somewhat

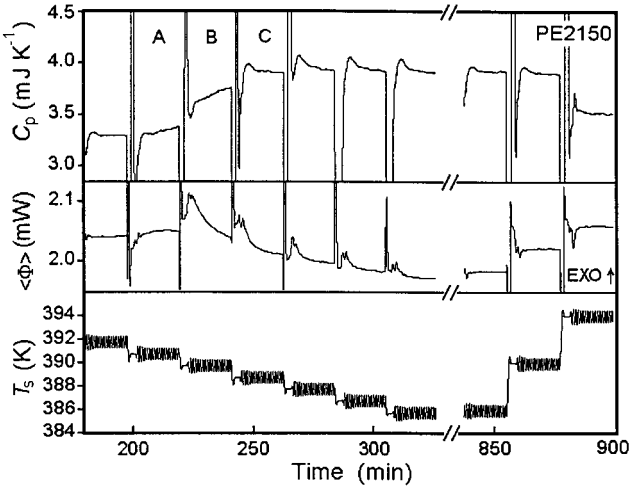

Figure 7. Detailed analysis in the region of the reversing melting peak of PE2150. Apparent reversing heat capacity, total heat-flow rate $\langle\Phi\rangle$, and sample temperature $T_s(t)$ during cooling and subsequent heating in the first crystallization steps and at the melting peak. A to C indicate runs that can be used for the study of crystallization.

higher, as is observed more prominently for PE560 in Figure 3. The maximum on first heating is higher for both fractions than on second heating and on cooling. The initial crystals melt during the first heating sequence and then crystallize into better crystals on subsequent cooling, due to the slower quasi-isothermal heating and cooling experiments. The better crystals melt on the subsequent second heating with a retracing of the reversing C_p of the prior cooling experiment. The magnitude of the small amount of apparent reversing C_p in the melting range is similar to that found for other polymers.[14−17] At low temperature, the expected heat capacity without latent heat contributions is reached only at about 300 and 270 K, respectively; i.e., a small amount of reversing melting and crystallization exists even below room temperature. This increase in heat capacity below room temperature is known from standard calorimetry for almost 40 years.[31] It increases substantially with decreasing crystal perfection, as could be studied recently by an extensive analysis of poly(ethylene-*co*-octene-1).[32,33]

Figure 7 displays for PE2150 more details about the crystallization (cooling) and melting (second heating) in the time domain, using graphs for the modulation of the temperature (bottom), the total heat flow rate (middle), and the apparent, reversing, specific heat capacity (top). The run is similar, but not identical, to the one shown in Figure 6. At the initial crystallization (marked A), $\langle\Phi\rangle$ reaches an almost constant, but slightly elevated, exothermic level, while the apparent reversing heat capacity increases continuously. Next, at temperature B, the total heat flow rate $\langle\Phi\rangle$ decreases from a strongly exothermic level, while the reversing C_p continues to increase. At point C and lower temperatures, both $\langle\Phi\rangle$ and the reversing C_p decrease. These changes will be discussed below on hand of the raw data of the heat flow rate and compared to the lower and higher molar mass materials.

TMDSC of PE15520. Figure 8 represents the results for PE15520. Again, the thick, continuous solid line is the apparent total C_p by standard DSC at 10 K min^{-1}, carried out prior to the quasi-isothermal TMDSC measurements. The open circles are the apparent reversing C_p, obtained from the quasi-isothermal heating TMDSC.

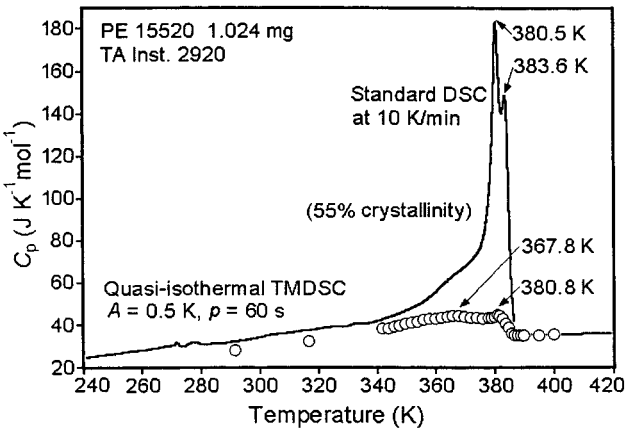

Figure 8. Apparent heat capacities measured by standard DSC and quasi-isothermal TMDSC for PE15520 crystallized first from the melt on cooling at 10 K min^{-1}. The solid line is obtained by standard DSC at 10 K min^{-1} and the open circles represent the apparent, reversing heat capacity by quasi-isothermal measurements.

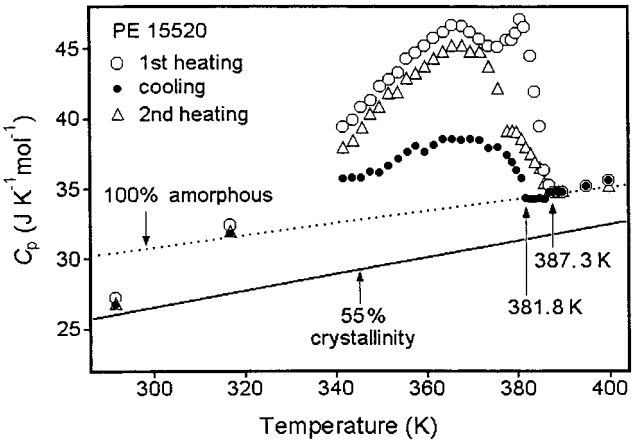

Figure 9. Apparent, reversing heat capacities of PE15520 on heating and cooling by quasi-isothermal TMDSC. Open circles, filled circles, and triangles represent the first heating, the subsequent cooling, and the second heating, respectively (compare to Figure 8).

The crystallinity determined from the heat of fusion measured by standard DSC is 55%. On the standard DSC trace, there are two peaks which are close to each other. The second peak commonly results from better crystals which form during perfection of initially poor crystals by annealing during heating for analysis as discussed in detail in the past.[3] In the apparent, reversing C_p trace, the two peaks merge to one very small peak at 380.8 K. There is also a very broad, shallow maximum at 367.8 K which seems to correspond to the shoulder at 370 K in the standard DSC trace. Overall, the quasi-isothermal, apparent reversing heat capacity covers only a small part of the total melting peak but extends to low temperature. Melting and crystallization is thus largely irreversible with an extended low-temperature, reversing contribution.

Figure 9 shows again the enlarged and additional TMDSC traces. The double peak by standard DSC in Figure 8 at about 380 K and showing as a single peak on first heating by TMDSC is barely visible on cooling and second heating. A second cooling run is identical to the first and not plotted in Figure 9. The end of melting on first and second heating is at 387.3 and 386.8 K, respectively, and the onset of crystallization on first and second cooling is at 381.8 K. The difference of about

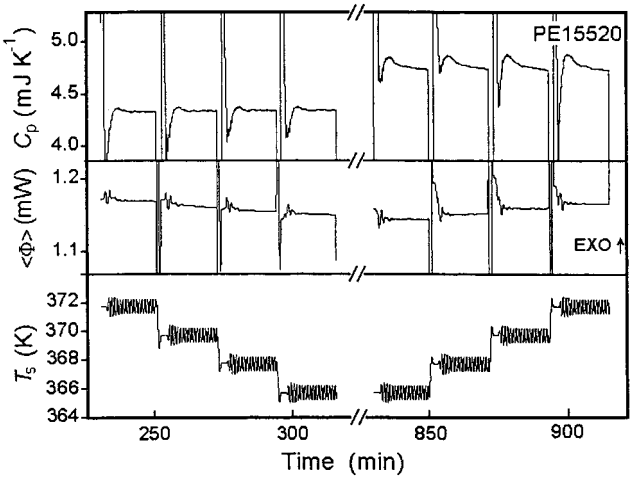

Figure 10. Detailed analysis in the region of the reversing melting peak of PE15520. Apparent reversing heat capacity, total heat-flow rate $\langle\Phi\rangle$, and sample temperature $T_s(t)$ during cooling and subsequent heating in the region of the melting peaks.

5.5 K is the supercooling of PE15520. The dotted line represents a 100% amorphous sample, as given in the ATHAS data bank,[30] and the solid line is for the expected heat capacity for a sample of 55% crystallinity, as was determined by standard DSC, measured after all quasi-isothermal TMDSC runs were completed.

The reversing C_p measured on first heating has higher values than on second heating over the entire temperature range. On cooling, the reversing heat capacity is much lower. For the first effect, it is assumed that the initially poorer crystals melt during the first heating sequence and then recrystallize to higher perfection on subsequent cooling, due to the slower cooling in the TMDSC experiments. These better crystals anneal less on subsequent heating, eliminating the peak at 380 K, but show, otherwise, a similar apparent reversing heat capacity as the first heating. Of further interest is the much higher C_p on heating than on cooling, in contrast to PE1150 and PE2150 (see Figure 6) and to PE560 (see Figure 3). Integrating the reversing heat capacity over the whole melting range leads to less than 10% reversing crystallinity for the cooling runs, but note that such integrations are usually not quantitative and may, due to slow processes, overestimate the truly reversible crystallinity.

Figure 10 displays, as before, more details about the crystallization and melting, using graphs for the modulation of the temperature (bottom), the total heat flow rate (middle), and the apparent, reversing heat capacity (top). The points chosen for analysis are in the temperature region of the broad peak of the cooling data of Figure 9. In the given scale all values of $\langle\Phi\rangle$ are constant with time after attainment of instrumental steady state. The reversing C_p on cooling also changes only little, but in the heating sequence, it starts at higher values and decreases with time. Therefore, the gap of reversing C_p between heating and cooling run decreases, but on extrapolation to longer times does not reach equal levels.

Discussion

This research was originally designed to be carried out entirely with *n*-paraffins with lengths that ultimately would exceed the length for chain folding. With such materials, the effects seen in multicomponent systems could be avoided, simplifying the interpretation

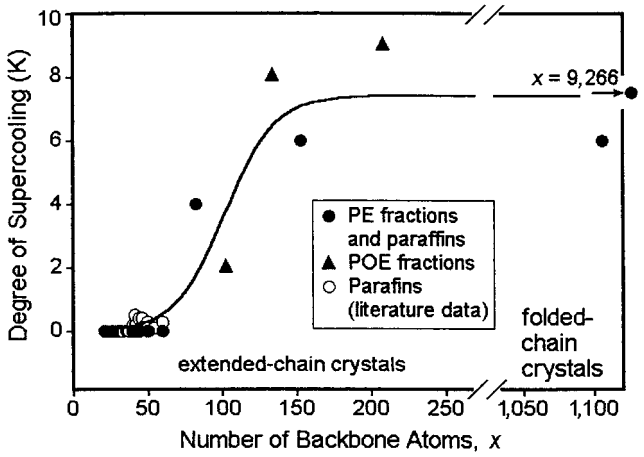

Figure 11. Degree of supercooling as a function of the number of chain atoms in the backbone of the materials listed in Table 1. Open circles are paraffin data from the literature.[21]

of the data. It is well-known that paraffins of different chain length as well as polymer fractions below molar masses of about 20 000 Da can undergo eutectic phase separation on crystallization.[3] Sufficiently long paraffins were produced in the past in Great Britain with support of their Engineering and Physical Research Council (EPSRC). Our request for samples, known to be available, was denied because "universally and without exception" EPSRC imposed the condition that "no material must leave the country". Naturally, we are of the opinion that fundamental research will be impeded when national interests limit exchange of information. Fortunately, our sample PE560 is sufficiently similar in its crystal nucleation behavior to the earlier studied *n*-paraffins up to $C_{50}H_{102}$, that major parts of the research did not have to be abandoned. The surprising finding that *n*-paraffins practically do not need primary, secondary, or molecular nucleation up to considerable lengths in typical experimental environments carries over into oligomer fractions generated out of polymers as shown in Figure 1.

Critical Length for Nucleation. In Figure 11 data are given to answer the question of how long must a molecule be before a noticeable nucleation barrier exists for crystallization under typical DSC conditions? The data of Figure 11 include information on all oligomers and polymers listed in Table 1 and some additional literature data on paraffins.[21−23] The crystals to the left of the break are of the extended-chain type. The points to the right refer to folded-chain crystals. It is clearly seen that there is a critical region for the backbone atoms at which molecular nucleation (or secondary nucleation) starts to be important for the description of the crystal growth, centered at 100 backbone atoms or about 12.5 nm of chain length. This point is much less than the 37 nm which is the critical chain length for *n*-paraffin to chain-fold[28,29] under similar crystallization conditions. An extensive DSC analysis of crystallization and melting of polyethylene of a much higher mass average of 130 000 Da and a polydispersity of 13 was made earlier in the presence and absence of equilibrium crystal seeds. The approximate of supercooling for the initial growth of chain-folded crystals on a similar time scale than for the present experiments was 7.5 K below the zero-entropy production melting temperature, in good agreement with Figure 11.[1] The poly(oxyethylene) oligomers fit onto the same graph with PE oligomers, an indication that the similarly flexible POE crystallizes as PE does.

Comparison of PE560 with Paraffins. The $C_{50}H_{102}$, $C_{44}H_{90}$, and $C_{26}H_{54}$ paraffins listed in Table 1 were analyzed previously with DSC and TMDSC.[19,20] The paraffins $C_{44}H_{90}$ and $C_{50}H_{102}$ show only a single, largely reversible melting transition, as expected from the well-known fact that *n*-paraffins above $C_{36}H_{74}$ exhibit only one crystal phase, while $C_{26}H_{54}$ falls into the group of paraffins between $C_{21}H_{44}$ and $C_{36}H_{74}$, which display a disordering transition to a mesophase below T_m in addition to the melting transition. The melting transition is in this case is called an isotropization since the mesophase can be considered to be already "partially melted".[34] The PE560 oligomer whose mass and number-average lengths correspond to $C_{40}H_{82}$ and $C_{37}H_{76}$, respectively, shows two transition peaks. In a recent reference,[21] the mesophase transition was detected up to $C_{37}H_{76}$. The peak on TMDSC and the shoulder on DSC at about 333 K in Figure 2 might, thus, contain contributions from the mesophases of $C_{37}H_{76}$ and shorter chains, as observed in $C_{26}H_{54}$.[20] The main part of the melting peak at 333 K, as well as the broadening of the melting range, however, should be caused by the eutectic phase behavior, known to occur on well-crystallized melts of paraffins of different lengths.[3]

To understand typical eutectic phase diagrams in paraffins, the eutectic temperature of the PE560 system can be analyzed using the Flory−Huggins equation or its extension to multicomponent systems.[35] A eutectic point at 1.3 K below $T_m°$ of PE560 was calculated for a PE560/$C_{50}H_{102}$ solution assuming $\chi = 0$. For PE560/$C_{37}H_{76}$ this difference increased to 7 K and for PE560/$C_{26}H_{54}$ to 25 K. Therefore, a broadened eutectic can easily contribute to the secondary peak in Figure 2 at 10 K below the main melting peak. Experimental data of extended-chain crystals of polyethylene of a weight-average molar mass of 2550 Da and a polydispersity of 1.6, much larger than in PE560, showed an even broader melting range with several lower temperature eutectic peaks,[36] while a phase diagram of a mixture of pure $C_{30}H_{62}$ and $C_{22}H_{46}$ has a melting range between the eutectic and the melting temperature of $C_{30}H_{62}$ of up to 24 K,[37] making the eutectic crystallization a likely cause for the broadening of the melting in PE560 of Figure 2.

As shown in Figures 2 and 8, the reversibly melting fraction of PE560 is much larger than for the high molar mass PE15520, and the biggest crystals in PE560 which melts last on heating also crystallize first on cooling without supercooling. Again, such behavior is expected from a eutectic phase diagram at equilibrium. On heating, the last crystals melting, and on cooling, the first crystals growing, both consist of the pure component of highest molar mass, as observed in Figure 3. Quite similar results were found on TMDSC of a sample of not quite pure $C_{44}H_{90}$.[20]

The quasi-isothermal measurements on paraffins with the much smaller modulation amplitude of ±0.05 K when compared to the present data in Figure 3 showed incomplete melting and crystallization in the temperature range of modulation due to limitations of the heat flow rate.[20] On raising the average temperature to next higher value of T_0, the crystals that should have melted, melted irreversibly at the new T_0 during the first few cycles until the new steady state was reached. In such cases the reversing heat flow rate is strongly asymmetric due to the larger melting contribution

during heating, and naturally, the first harmonic of this asymmetric response of the sample is not usable for a quantitative analysis. In the present analysis of PE560, these problems were largely avoided by choosing larger modulation amplitudes and helped by the inherently smaller amount of change in crystallinity over the much broader melting range. Figure 4 shows the practically constant apparent heat capacity at points g−i after reaching steady state. Every modulation cycle is symmetric in crystallization and melting, so that the overall progress of melting occurs when the temperature is increased from one quasi-isothermal T_0 to the next, and the amplitude of the apparent reversing heat capacity can be separated into a contribution due to the reversible thermodynamic heat capacity and the reversible latent heat exchanged on crystallization and melting as graphed in Figure 3. If measurements would have been carried out with an underlying heating rate $\langle q \rangle$ and not quasi-isothermally, the modulation amplitudes in successive cycles would overlap, and the integral reversible heat of fusion would erroneously exceed the total heat of fusion, as was demonstrated for the reversible melting of indium.[18]

Comparison of the Oligomers with Polyethylene. Although PE1150 and PE2150 are oligomers, they have a higher measured melting temperature than PE15520, as is seen in Figure 1. The melting temperatures of PE1150 and PE2150 are close their equilibrium melting temperatures, ensuring these samples consist of extended-chain crystals, as were also found for the paraffins and PE560 and expected from the well-established upper limit of 37 nm for extended-chain crystallization of paraffins at atmospheric pressure.[28,29] In contrast, PE15520 shows in Figure 9 an end of melting about 25 K below its equilibrium melting temperature. This agrees with a reasonable lamellar crystal thickness of about 10.5 nm, as can be calculated from an equation derived from a large number of data on the melting temperatures of polyethylenes of known lamellar thickness:[3]

$$L \text{ (in nm)} = 0.627 \frac{T_m^\circ}{T_m^\circ - T_m} \qquad (3)$$

where T_m is melting temperature of the folded-chain crystal, T_m° is the melting temperature of the extended chain crystal represented by eq 2, and L is the lamellar thickness. The analyzed samples, thus, have two different macroconformations and melting behaviors.[3]

On crystallization PE560 and the paraffins show no supercooling and crystallize largely reversibly; PE1150 and PE2150 show supercoolings of 4.1 and 5.8 K, respectively, values which are similar to that of PE15520 (5.5 K, see Figure 9) when basing the analysis on the zero-entropy production melting temperature, but basing the supercooling on its equilibrium melting temperature, the supercooling of PE15520 is much larger. It is interesting to note that the much higher molar mass PE130000, when crystallized at about 400 K at times comparable to the present DSC experiments, yields lamellar crystals of about double the fold length,[5] but with only little larger supercooling (7.5 K) from the zero-entropy production melting temperature, while its supercooling from the equilibrium melting temperature is half that of the PE15520 (30.1 vs 14.3 K, respectively).

Comparing the shape of the melting curves by standard DSC in Figures 2, 5, and 8, one finds the broadest melting peak for PE560 (≈50 K), a narrower peak for PE1150 (≈30 K), and the narrowest for PE2150 (≈20 K) and a broad peak of about 40 K with a superimposed sharper peak of about 20 K for PE15520. The analysis of the reversing melting reveals a beginning deviation from the heat capacity originating from vibrations only at 260−280 K for all samples, only a little above the glass transition. For PE560 this early deviation is fully reversible, as found earlier for the paraffins.[38] The first separation between reversing and total C_p is seen at 330 K, well into the melting peak, at an apparent heat capacity of ≈95 J K^{-1} mol^{-1} (see Figure 2). For PE1150 and PE2150, the first separation between total and reversing heat capacity occurs at 360 and 380 K, respectively, just before major melting commences, at an apparent C_p of about 40 J K^{-1} mol^{-1} (see Figure 6), while for PE15520 this separation is seen over the whole temperature region between glass transition and melting, starting at about 260 K, at an apparent C_p of about 25 J K^{-1} mol^{-1} (see Figures 8 and 9). For all three samples, PE1150, PE2150, and PE15520, the apparent reversing heat capacity reaches the level of the heat capacity of the melt before major melting has begun. These observations point to a continuous change in the mechanism of reversing melting when going from paraffins to polymer. While all samples have a basic increase in heat capacity beyond that of the vibrational contribution which was linked to a fully reversible conformational motion within the crystals, based on a combined discussion of computer simulations, infrared data, and heat capacity measurements,[39] only polyethylene PE15520 shows a small amount of irreversible melting beginning at the glass transition, followed by an additional reversing melting in the melting peak region (see Figures 8 and 9); the oligomers show an increasing amount of reversible melting with decreasing molar mass.

The next topic concerns the reversing portion of the melting beyond that of the conformational motion which can increase the apparent heat capacity at best to the level of the liquid, the level of full conformational mobility. Figures 3, 6, and 9 are the basis for this discussion. The PE560 was linked to the reversible melting of the paraffins within the range of modulation amplitude. The remaining irreversible part is expected to be connected to the incomplete separation of the various species on crystallization, as is seen on cooling at temperatures a−f in Figure 4 and discussed in the next section on the kinetics. The PE1150 and PE2150 are characterized by decreasing amounts reversible melting, as was also seen for oligomers of poly(oxyethylene)s in the same molar mass range (POE1500 to POE5000).[16,17] The remaining reversible increase in heat capacity seems to be largely truly reversible since the quasi-isothermal reversing heat capacities are independent of time (see Figure 7). The polymer PE15520 behaves quite differently. The reversing contribution to the melting peak is larger than for PE2150 when one considers that the crystallinity is little more than half that of PE1150 or PE2150 (compare Figures 6 and 9). To discuss more of the details of the small amount of reversing melting and to assess the truly reversible fraction, the possible annealing of the sample must be eliminated, as is done in the next section. The large difference between reversing heat capacity on cooling and on heating shown in Figure 9 indicates that as much as half of the material contributing to the reversing melting crystallizes irreversibly at lower tempera-

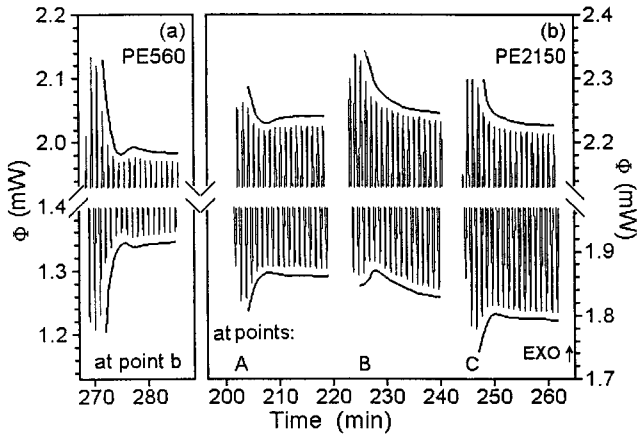

Figure 12. Raw heat-flow rate data $\Phi(t)$ as a function of time. (a) Data for PE560 as a function of time for point b in Figures 3 and 4. (b) Data for PE2150 as a function of time for points A, B, and C in Figure 7. The center area is omitted to be able to increase the ordinate. The solid line is drawn somewhat above the endothermic and exothermic maximum amplitudes for clarity.

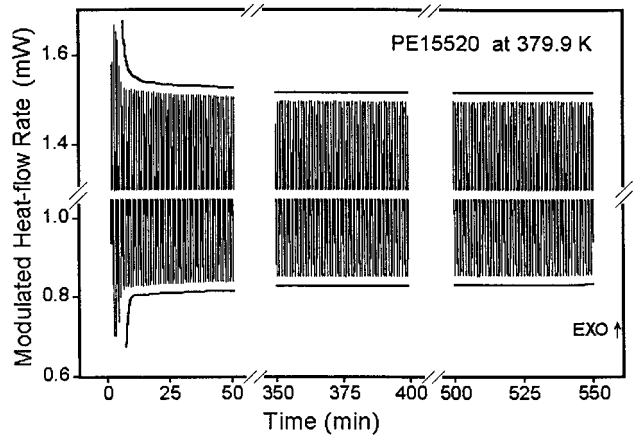

Figure 13. Raw heat-flow rate data $\Phi(t)$ for PE15520 as a function of time from a long-time quasi-isothermal experiment at 379.94 K at the high-temperature peak of a sample of specially poor crystallization history. Shown are excerpts at 0−50, 350−400 and 500−550 min. The center areas are omitted to be able to increase the ordinate. The solid line is drawn somewhat above the endothermic and exothermic maximum amplitudes for clarity.

tures. This is different from PE2150, which grows all reversibly melting species close to its melting temperature after the initial supercooling, while PE560 and to a lesser degree also PE1150 has a larger reversing C_p on cooling.

Kinetics of the Processes Seen by TMDSC. The kinetics of the changes in the quasi-isothermal analysis in terms of the apparent, reversing heat capacity and the total heat flow rate is shown in Figures 4, 7, and 10. Figures 12 and 13 add the actual raw data in the time domain of the heat flow rate for selected temperatures for PE560, PE2150, and PE1550 in order to judge the symmetry of the response to the modulation and find causes for the nonreversing contributions.

For PE560 much of the response is reversible within the parameters of modulation. The larger apparent total heat capacity of the final melting peak in Figure 2 is linked to the kinetics of the processes which may arise not so much from lags of the calorimeter, but from slow kinetics to reach equilibrium within the sample by diffusion and selection of the various species attaining equilibrium only at the proper crystal thickness. The instrument-caused effects have been seen in earlier work on pure paraffins, analyzed with a different calorimeter using sawtooth modulation.[20] The missing reversing heat of fusion was in the latter cases evolved during the heating from one base temperature to the next and at the melting peak also in the first few modulation cycles at the higher temperature. With the present instrumentation, no recording of the heat flow rate is possible between runs, but we assume that it may occur, although only to a smaller degree. The melting range of PE560 is sufficiently broad, so that no additional melting at the higher temperature can be distinguished during the approach to steady state as seen, for example, in Figure 12a during the time up to 277 min. Reversible low-latent-heat transitions of liquid crystals where similarly analyzed.[40] Temperature lags in the sample pan could also be documented directly by contact-less measurements within the DSC cell by infrared thermography.[41]

Slow, irreversible processes within the sample of PE560 can be seen from the decrease of the reversing heat capacity with time in the cooling sequence f−a of Figure 4. It was suggested in the discussion, above, that this decrease in reversing heat capacity may, in time, reach agreement with the quasi-isothermal experiments on heating (sequence g−i). Approximately 100 min should be sufficient to reach such true equilibrium. Figure 12a indicates a largely symmetrical heat flow rate, but from 277 to 287 min into the experiment, after attainment of steady state, the amplitude of the endothermic cycle decreases faster than the exothermic one. This observation indicates that in every cycle a small amount of the recrystallized material achieves a sufficiently higher melting point due to better crystal perfection to fall outside the temperature range covered on the subsequent heating. Similar decreases in apparent reversing heat capacity are seen also in polymers on annealing. Examples are seen in homogeneous poly(ethylene-*co*-octene)s on annealing in the melting range of sequences of paraffinic lengths[32,33] and on annealing of poly(ethylene terephthalate) in the melting region.[14,15]

The analysis of the PE2150 in Figure 5 shows that its melting is largely irreversible. The small reversing contribution to the apparent heat capacity develops to a peak of 10 J K^{-1} mol^{-1}, as seen in Figure 6. Figure 7 reveals that, except for temperatures A, B, and C, little changes occur in the apparent reversing heat capacities with time; i.e., the effect has reversible causes. The small irreversible peaks like the one at 370 K and the increased reversing peak at 390 K disappear from the reversing heat capacity on more careful crystallization, an indication that poorer crystallization increases the apparent reversing heat capacity. Quite similar increases in apparent reversing heat capacity were observed for POE with molar masses of 1500 and 5000 Da and most other polymers analyzed to date.[18,42] Their existence has been linked to surface melting either on fold surfaces[43,44] or on side surfaces.[14,45]

The kinetic effect at points A, B, and C, in Figure 7, which represent the initial temperatures of crystallization, may shed some light on the development of the reversing melting on crystallization. At the point A in Figure 7, one observes the first linear increase in the apparent reversing heat capacity. It starts only after steady state is reached, and the total heat flow rate is slightly more exothermic than the response of the melt,

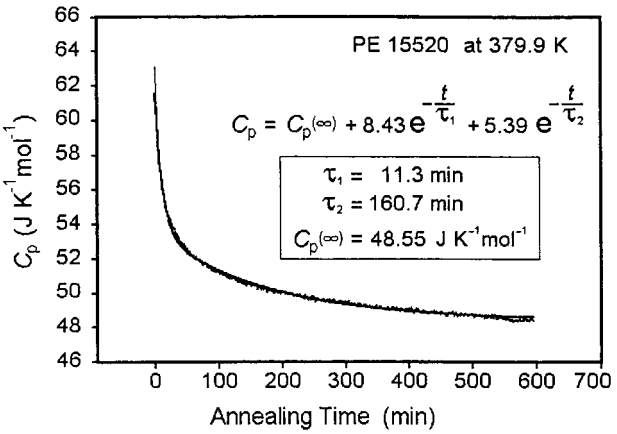

Figure 14. Plot of the change in apparent, reversing heat capacity for the data of Figure 13 as a function of annealing time.

indicating a constant rate of crystallization starts slightly earlier and causes a continuing linear increase in reversibly melting material. Figure 12b shows at the temperature A that the amplitude of the response to modulation is largely symmetric with slight increases in the exotherm. The endotherm increases also, but only half as much; i.e., about half of the added crystallization in each cooling cycle is melted again in the subsequent heating. Full reversibility is not reached in the time of analysis. At temperature B, the increase in apparent reversing heat capacity continues and reaches a constant level at C (see Figure 7). The total heat flow rate, in turn, is much different. A large, irreversible crystallization exotherm that decreases with time and is less in each subsequent analysis step is superimposed on the modulation effect, as seen in Figures 7 and 12b. At temperature B, the reversing heat flow rate, again, is largely symmetric and increases in B somewhat by increasing the exotherm slightly more than the endotherm in successive steps. In C there is hardly any asymmetry detectable and, judging from the total heat flow, by this time the bulk of the irreversible crystallization has taken place. The reversible crystallization stays constant for several more steps of cooling before decreasing but reaches zero only close to the glass transition. Below about 370 K the total and reversing apparent heat capacities are equal, which means that all of the early melting is reversible.

The polymer PE15520 behaves different again. The low-temperature reversing melting is, in this case, only partially reversible, and the fraction of reversing apparent heat capacity is more than in PE2150 and is larger in the poorly crystallized sample (see Figures 8 and 9). Figure 10 shows that on cooling the reversing apparent heat capacity is constant with time, while on heating it is larger and decreases with time. The explanation for this increased reversing melting in the heating experiment may be that the material causing the increase was grown at lower temperature during the cooling as secondary crystals in a matrix of the primary crystals. These initially rather poor crystals are the subject of annealing after crystallization and melt on reheating at higher temperature. Within the frame of the metastable primary crystals they may also reach in time a reversible local melting. Figures 13 and 14 illustrate the changes at 379.9 K in a long-time experiment for a sample with an even larger peak in the reversing, apparent heat capacity than shown in Figure 9. The ultimately reached level of reversing heat capacity of 48.55 J K^{-1} mol^{-1} is still much above the constant level reached on cooling. As for all other polymers of high molar mass that have been analyzed in this fashion, two processes seem to be involved in the kinetics with the indicated relaxation times. Both times are longer than the response of the calorimeter, and Figure 13 indicated that the short-time change is based on a faster changing exotherm. Otherwise, the decrease in the heat flow rate is largely symmetric. One expects, thus, that an annealing process is involved in the decrease of the reversing heat capacity which starts with a small exotherm of crystal perfection. Each perfected crystal is then is removed from the subsequent melting cycle. Similarly, a fully melted molecule would be removed from the reversing melting since it would need a renewed molecular nucleation to recrystallize. It takes several hundred minutes until this process reaches a steady state and can be considered a true local equilibrium in the matrix of the metastable crystals.

Conclusions

Quantitative calorimetry supported by temperature-modulated calorimetry opens the possibility to gain considerable new insight into the crystallization and melting of polymers. Of special importance is the observation that there exists a narrow range of chain lengths below which paraffinic and related flexible chain molecules act like small molecules and can melt reversibly in the presence of heterogeneous nuclei (see Figure 11). For paraffins, polyethylene, and its oligomeric fractions, this range centers around a critical chain length of about 100 chain atoms. This corresponds to a chain length of about 12.5 nm, a molar mass of about 1400 Da, and an equilibrium melting temperature of about 385 K. A similar relationship may holds for poly(oxyethylene), which represents a similarly flexible macromolecule.

The observed increase of the apparent reversing heat capacity in the melting range of polyethylene, its oligomers, and paraffins can be related to one or more of three causes:

(1) A gauche−trans equilibrium within the crystals. Using the known heat capacity contribution of the density of vibrational states as a quantitative baseline, it is seen that a slow increase of the heat capacity of the crystals starts at about 250 K. The cause of this increase was documented for paraffins[38] and polyethylene[30,31] and is linked to the introduction of gauche defects into the crystals which collect at higher concentrations at the chain ends or fold surfaces.[39] The main increase in heat capacity is the potential energy increase caused by the addition of the gauche defects. It may be possible that the earlier observed reversible increase of lamellar thickness[46,47] has the same cause.

(2) Equilibrium melting and crystallization of paraffinic crystals. These paraffins melt reversibly at a temperature that can be estimated from eq 2, modified by the changes of multicomponent systems, as described by the Flory−Huggins formalism.[35,36] It must be remembered in this connection that chain ends (cilia) or segments connected on both ends to polymer crystals can act as paraffins when given sufficient mobility, as was shown for polymers with sufficiently long side chains.[3]

(3) Partially melted polymer segments that remain attached to polymer crystals. These were identified by their inability to be removed physically after melting[48]

and may be able to crystallize and melt reversibly without the need to go through a molecular nucleation process. This is most likely the major contribution in the high-temperature reversible melting peaks of polymers since the melting temperatures judged by eq 2 reach in this case the chain lengths which change from small molecule to polymer behavior of Figure 11. Since global equilibria do not exist in the melting region of polymers, the reversible processes must take place locally within a metastable structure, set up by the main body of the interconnected crystals of the macromolecules. Other components of this metastable structure are the mobile− and rigid−amorphous fractions[49] that can also be studied by TMDSC.[50]

The study of the kinetics of changes of the reversing heat capacity allows the separation of annealing processes from truly reversible processes, even in the presence of fully irreversible crystallization. The best means to study the irreversible behavior is to compare separate standard DSC data which yield the total, apparent heat capacity data with the reversing data from quasi-isothermal measurements, as shown in Figures 2, 5, and 8. The quasi-isothermal analyses permit the identification of instantaneous processes relative to the time scale of calorimetry as well as slower processes as shown in Figures 4, 7, 10, 12, and 13.

To summarize the results of the four different samples analyzed in this paper, only PE560 approaches equilibrium and much of its reversible melting can be explained by effects (1) and (2), in addition to the possible existence of mesophase transitions for the lower molar mass fractions and some irreversible effects due to instrument lag and sample kinetics (diffusion and recrystallization). Practically all chain lengths of its components are below the critical chain length of Figure 11. The crystals of PE1150 and PE2150 are also of the extended chain nature as are the paraffins, but the molecular lengths are within the range of change form reversible to irreversible melting of Figure 11. These two samples have the most completely irreversible melting and crystallization behavior of the four samples. All increases in the apparent reversible heat capacity at low temperatures beyond that of the vibrational contribution are probably of cause (1). The true reversibility of PE560 changes increasingly from cause (2) to cause (3) (peaks in Figure 6). In the polymer PE15520, the apparent, reversing heat capacity increases and stretches over a wider temperature range. At low temperature it is less than the total heat capacity; i.e., the effect (1) is mixed with some irreversible melting or annealing and possibly contains some reversible melting of small paraffinic crystals (2) as seen to a much larger extent in the poly(ethylene-*co*-octene)s.[32,33] The final, small amount of reversing melting above about 380 K, again, is expected to result from cause (3).

Obviously these assignments are only one of the first attempts to separate the various reversible processes between the glass and the melting transition. It is obvious that the limit of the TMDSC method has not been reached. Further work coupled with more specific morphological studies can give additional insights. For example, reversible effects described at the fold surface of polyethylene[43] must still be separated quantitatively from possible additional side-surface effects as are expected from the molecular nucleation and proven, for example, for polypropylene,[45] which shows no reversible effects on the fold surface. Finally, the possible complication from rigid amorphous fractions can be separated, removing a complication of particular importance for the stiffer polymer chains, as shown for polycarbonate.[50]

Acknowledgment. This work was supported by the Division of Materials Research, National Science Foundation, Polymers Program, Grant DMR-9703692, and the Division of Materials Sciences, Office of Basic Energy Sciences, U.S. Department of Energy at Oak Ridge National Laboratory, managed and operated by UT-Batelle, LLC, for the U.S. Department of Energy, under Contract DOE-AC05-00OR22725.

References and Notes

(1) Wunderlich, B.; Cormier, C. M. *J. Phys. Chem.* **1966**, *70*, 1844.
(2) Wunderlich, B. *Macromolecular Physics;* Academic Press: New York, 1976; Vol. 2.
(3) Wunderlich, B. *Macromolecular Physics;* Academic Press: New York, 1980; Vol. 3.
(4) Wunderlich, B. *Polymer* **1964**, *5*, 611.
(5) Wunderlich, B. *Macromolecular Physics;* Academic Press: New York, 1976; Vol. 1.
(6) Wunderlich, B.; Mehta, A. *J. Polym. Sci., Polym. Phys. Ed.* **1974**, *12*, 255.
(7) Mehta, A.; Wunderlich, B. *Colloid Polym. Sci.* **1975**, *253*, 193.
(8) Cheng, S. Z. D.; Bu, H. S.; Wunderlich, B. *J. Polym. Sci., Part B: Polym. Phys.* **1988**, *26*, 1947.
(9) Cheng, S. Z. D.; Wunderlich, B. *J. Polym. Sci., Part B: Polym. Phys.* **1986**, *24*, 577.
(10) Wunderlich, B. *Discuss. Faraday Soc.* **1979**, *68*, 239.
(11) Reading, M.; Elliot, D.; Hill, V. L. *J. Therm. Anal.* **1993**, *40*, 949.
(12) Gill, P. S.; Sauerbrunn, S. R.; Reading, M. *J. Therm. Anal.* **1993,** *40*, 931.
(13) Reading, M. *Trends Polym. Sci.* **1993**, *8*, 248.
(14) Okazaki, I.; Wunderlich, B. *Macromolecules* **1997**, *30*, 1758.
(15) Okazaki, I.; Wunderlich, B. *Macromol. Chem. Phys., Rapid Commun.* **1997**, *18*, 313.
(16) Ishikiriyama, K.; Wunderlich, B. *Macromolecules* **1997**, *30*, 4126.
(17) Ishikiriyama, K.; Wunderlich, B. *J. Polym. Sci., Part B: Polym. Phys.* **1997**, *35*, 1877.
(18) Wunderlich, B.; Boller, A.; Okazaki, I.; Ishikiriyama, K.; Chen, W.; Pyda, M.; Pak, J.; Moon, I.; Androsch, R. *Thermochim. Acta* **1999**, *330*, 21.
(19) Pak, J.; Boller, A.; Moon, I.; Pyda, M.; Wunderlich, B. *Thermochim. Acta* **2000**, *357/358*, 259.
(20) Pak, J.; Wunderlich, B. *J. Polym. Sci., Part B: Polym. Phys.* **2000**, *38*, 2810.
(21) Kraack, H.; Sirota, E. B.; Deutsch, M. *J. Chem. Phys.* **2000**, *112*, 6873.
(22) Kraack, H.; Deutsch, M.; Sirota, E. B. *Macromolecules* **2000**, *33*, 6174.
(23) Sirota, E. B. *Langmuir* **1998**, *13*, 3133.
(24) Wunderlich, B.; Jin, Y.; Boller, A. *Thermochim. Acta* **1994**, *238*, 277.
(25) Buckley, C. P.; Kovacs, A. J. *Prog. Colloid Polym. Sci.* **1975**, *58*, 44.
(26) Boller, A.; Okazaki, I.; Ishikiriyama, K.; Zhang, G.; Wunderlich, B. *J. Therm. Anal.* **1997**, *49*, 1081.
(27) Broadhurst, M. G. *J. Chem. Phys.* **1962**, *36*, 2578.
(28) Bassett, D. C.; Olley, R. H.; Sutton, S. J.; Vaughan, A. S. *Macromolecules* **1996**, *29*, 1852.
(29) Bassett, D. C.; Olley, R. H.; Sutton, S. J.; Vaughan, A. S. *Polymer* **1996**, *37*, 4993.
(30) Wunderlich, B. The Athas Data Base on Heat Capacities of Polymers. *Pure Appl. Chem.* **1995**, *67*, 1919. For data see the Internet address web.utk.edu/~athas/databank.
(31) Wunderlich, B. *J. Chem. Phys.* **1962**, *37*, 1203.
(32) Androsch, R.; Wunderlich, B. *Macromolecules* **1999**, *32*, 7238.
(33) Androsch, R.; Wunderlich, B. *Macromolecules* **2000**, *33*, 9076.
(34) Wunderlich, B.; Grebowicz, J. *Adv. Polym. Sci.* **1984**, *60/61*, 1.
(35) Prime, R. B.; Wunderlich, B. *J. Polym. Sci., Part A2* **1969**, *7*, 2073.
(36) Prime, R. B.; Wunderlich, B.; Melillo, L. *J. Polym. Sci., Part A2* **1969**, *7*, 2091.
(37) Nechitailo, N. A.; Topchiev, A. V.; Rozenberg, L. M.; Terentava, E. M. *Zh. Fiz. Khim.* **1960**, *34*, 1268.

(38) Jin, Y.; Wunderlich, B. *J. Phys. Chem.* **1991**, *95*, 9000.
(39) For a detailed discussion of this topic see: Sumpter, B. G.; Noid, D. W.; Liang, G. L.; Wunderlich, B. Atomistic Dynamics of Macromolecular Crystals. *Adv. Polym. Sci.* **1994**, *116*, 27.
(40) Chen, W.; Dadmun, M.; Zhang, G.; Boller, A.; Wunderlich, B. *Thermochim. Acta* **1998**, *324*, 87.
(41) Androsch, R.; Pyda, M.; Wang, H.; Wunderlich, B. *J. Therm. Anal. Calorim.* **2000**, *61*, 661.
(42) Wunderlich, B.; Pyda, M.; Pak, J.; Androsch, R. *Thermochim. Acta*, to be published.
(43) Goderis, B.; Reynaers, H.; Mathot, V. B. F.; Scherrenberg, R.; Koch, M. H. J. *Macromolecules* **2001**, *34*, 1779.
(44) Hu, W.; Albrecht, T.; Strobl, G. *Macromolecules* **1999**, *32*, 7548.
(45) Androsch, R.; Wunderlich, B. *Macromolecules*, in press.
(46) Strobl, G. R.; Schneider, M. J.; Voigt-Martin, G. J. *Polym. Sci., Polym. Phys.* **1980**, *18*, 239.
(47) Tanabe, Y.; Strobl, G. R.; Fischer, E. W. *Polymer* **1986**, *27*, 1147.
(48) Mehta, A.; Wunderlich, B. *Makromol. Chem.* **1974**, *175*, 977.
(49) Suzuki, H.; Grebowicz, J.; Wunderlich, B. *Br. Polym. J.* **1985**, *17*, 1.
(50) Schick, C.; Wurm, A.; Merzyakov, M.; Minakov, A.; Marand, H. *J. Therm. Anal. Calorim.*, in press.

MA010195A